Magnetic and superconducting properties of single-crystal $TmNi_2B_2C$

B. K. Cho, Ming Xu, P. C. Canfield, L. L. Miller, and D. C. Johnston
Ames Laboratory and Department of Physics and Astronomy, Iowa State University, Ames, Iowa 50011-3020
(Received 9 March 1995)

The temperature (T) and applied magnetic field ($\mathbf{H}$) dependent magnetization has been measured for a single crystal of $TmNi_2B_2C$ in order to study the interplay of superconductivity and the magnetism of the Tm sublattice. The normal-state magnetization of $TmNi_2B_2C$ is anisotropic from 2 to 300 K with the magnetic field applied normal to the c axis ($\mathbf{H}\perp c$) leading to a smaller induced magnetization than the magnetization for the magnetic field applied parallel to the c axis ($\mathbf{H}\|\mathbf{c}$). This anisotropy is attributed to crystalline electric field (CEF) splitting of the $J=6$ manifold of the Tm^{+3} ion. From the inverse susceptibility $[1/\chi(T)]$ for $\mathbf{H}\|\mathbf{c}$ and $\mathbf{H}\perp\mathbf{c}$, the CEF parameter, B_2^0, is found to be (-1.15 ± 0.02) K. The superconducting state magnetization for $H\approx H_{c2}(T)$ obeys the Ginzburg-Landau theory which is used to evaluate the upper critical magnetic field $H_{c2}(T)$ and $dH_{c2}/dT|_{T_c}$ values. The superconducting properties in this temperature region are similar to those of the nonmagnetic superconductor YNi_2B_2C, which has been shown to be an isotropic conventional type-II superconductor. For $T\leq 6$ K, $H_{c2}(T)$ shows highly anisotropic behavior: $H_{c2}^{\perp c}\approx 2H_{c2}^{\| c}$. For both $\mathbf{H}\|\mathbf{c}$ and $\mathbf{H}\perp\mathbf{c}$, $H_{c2}(T)$ reaches a broad maximum near 4 K and decreases as T approaches $T_N=(1.52\pm0.05)$ K, indicating the interplay between superconductivity and magnetism. The broad maximum in $H_{c2}(T)$ of $TmNi_2B_2C$ is likely a result of the increasing Tm sublattice magnetization at $H_{c2}(T)$ with decreasing temperature, rather than of antiferromagnetic fluctuations.

I. INTRODUCTION

The recent discovery of superconductivity in the quaternary intermetallic compounds $LnNi_2B_2C$ (Ln =Sc, Y, Lu, Tm, Er, Ho or Th),[1–3] has received great attention because these materials have a layered structure, anisotropic magnetic characteristics, and relatively high superconducting transition temperatures (17 K for Ln =Lu). The transition temperatures (T_c) of these quaternary compounds are among the highest for intermetallic boride systems known to date, including $T_c=12$ K in the $LnRh_4B_4$ (Ln =rare-earth element) system.[4] These nickel-boride quaternary superconductors are particularly interesting because they have a two-dimensional (2D) structure, with alternating layers of Ni_2B_2 and LnC,[5] which is reminiscent of the structure of high-T_c copper-oxide superconductors in which the two-dimensional nature leads to large anisotropies in the superconducting and in the normal-state properties.

There is strong evidence for the coexistence of superconductivity and local magnetic moment ordering below T_c in the (Ho, Tm, Er)Ni_2B_2C compounds from electrical resistivity,[6] specific-heat,[7] and magnetization[8] measurements. The specific-heat measurements on $TmNi_2B_2C$ show features consistent with antiferromagnetic (AF) ordering at Néel temperature $T_N=(1.52\pm0.05)$ K (Ref. 7) and superconductivity at $T_c\approx 11$ K. In addition, below T_N the specific-heat data were interpreted in terms of a ferromagnetic interaction between the Tm^{+3} ions within the 2D TmC planes and a relatively weak antiferromagnetic coupling between planes, with substantial magnetic anisotropy at low temperatures.[7] While resistivity measurements in zero applied magnetic field H indicate no reentrance into the normal state near $T_N=1.5$ K, the same measurements on polycrystalline samples in applied fields indicate the start of a suppression in H_{c2} for temperatures slightly above T_N.[6] Such features in H_{c2} for $T\approx T_N$ are consistent with the development of AF order below T_N.[9]

Recently, magnetization measurements were carried out on single crystals of YNi_2B_2C and $HoNi_2B_2C$.[8,10] For the YNi_2B_2C crystal, the Ginzburg-Landau (GL) and London theories describe the data fairly well and the GL parameter κ was found to be around 6–9, thus indicating a type-II superconductor. Based on magnetization and torque measurements, the YNi_2B_2C crystal is shown to be an isotropic superconductor.[10] For the $HoNi_2B_2C$ crystal, the data are not described well by the same GL and London theories because the interplay between Ho^{+3} magnetic moments and superconducting electron pairs is strong enough to dramatically affect the superconducting properties in the whole temperature range below T_c. The estimation of the upper critical field $H_{c2}(T)$ from magnetization versus temperature data gives anisotropic values for $\mathbf{H}\|\mathbf{c}$ and $\mathbf{H}\perp\mathbf{c}$ with a deep minimum near $T_N\approx 5$ K for both orientations.[8] YNi_2B_2C and $HoNi_2B_2C$ samples typify two contrasting cases found in the $LnNi_2B_2C$ series. The former is a nonmagnetic superconductor and the latter is a magnetic superconductor with the largest value of $T_N/T_c\approx 6/8$ in the $LnNi_2B_2C$ series. It is interesting to study the magnetization and superconductivity in $TmNi_2B_2C$ because this sample has a ratio $T_N/T_c\approx 1.5/11$ which is the smallest, finite, value in the $LnNi_2B_2C$ series. We will compare and contrast the properties of $TmNi_2B_2C$ to those of the YNi_2B_2C and $HoNi_2B_2C$ materials.

0163-1829/95/52(5)/3676(8)/$06.00

After a brief description of the crystal growth and other experimental procedures in Sec. II, the low-field superconducting state data will be presented in Sec. III. This will be followed by the normal-state magnetization data for both **H**||**c** and **H**⊥**c**. Then the superconducting magnetization for several different fields, obtained by subtraction of the normal-state paramagnetic magnetization from the observed magnetization, will be examined. Using these data, the GL theory is applied near T_c to determine $H_{c2}(T)$ values. Next, the observed $M(H)$ data are closely examined to obtain H_{c2} values for a broader range of temperatures. In addition, superconducting parameters, such as $dH_{c2}(T)/dT$, GL parameters (κ), and the anisotropy factor (γ) will be derived. We summarize and restate our conclusions in Sec. IV.

II. EXPERIMENTAL DETAILS

Single crystals of $TmNi_2B_2C$ were grown by a Ni_2B flux method[10] that yielded crystals with masses up to 700 mg and dimensions up to 1 cm×1 cm×0.1 cm. First a polycrystalline, arc-melted button of stoichiometric $TmNi_2B_2C$ is made from a mixture of high purity Tm (Ames Lab: 99.99%), Ni (99.99%), B (99.5%), and C (99.99%), followed by annealing under vacuum in a sealed quartz tube at 1050 °C for at least 12 h. The powder x-ray-diffraction (XRD) measurement performed on such a polycrystalline button shows most of the major peaks of the known structure of $TmNi_2B_2C$ and minor peaks of second phases including TmNiBC and Ni_2B. The annealed $TmNi_2B_2C$ button is then placed inside an Al_2O_3 crucible together with an approximately equal mass of Ni_2B pieces. The crucible is heated to 1500 °C and slowly cooled (10 °C/h), under a continuous flow of high purity argon, to 1200 °C. The crucible is then cooled to room temperature, and the crystals are removed from the flux. The shape of the as-grown crystals is that of a two-dimensional plate. Powder XRD measurements of pulverized single crystals show a single-phase pattern without any of the second phases seen in polycrystalline samples except for a small (2,1,1) peak from Ni_2B which remains on the surface of the crystal. The x-ray patterns of the crystal surfaces show that the as-grown crystals have the crystallographic c axis perpendicular to the plate surface. A 12 mg single crystal, with dimensions of roughly 2×2×0.35 mm, was selected for this study. Temperature and field-dependent static magnetization data were measured using a Quantum Design superconducting quantum interference device magnetometer. The field-cooled (FCW) and zero-field-cooled (ZFC) data in the superconducting state were obtained on warming after the magnet was quenched.

III. RESULTS AND DISCUSSION

A. Low-field superconducting transition

The magnetization versus temperature data in Figs. 1(a) and 1(b) show the flux expulsion (FCW) and magnetic shielding (ZFC) effects for **H**⊥**c** and **H**||**c** in a $TmNi_2B_2C$ crystal for an external magnetic field $H = 10$ G. These plots show a sharp superconducting transition with transition onset at 11 K, transition temperature (midpoint) $T_c = 10.8$ K, and transition width (10–90 % of full diamagnetic signal) of about 0.4 K. The FCW values of both directions at 2 K are 80% (40%) of perfect superconducting flux expulsion values for **H**⊥**c** (**H**||**c**) and the ZFC ones are 150% (420%) without correction for demagnetization effects, indicating bulk superconductivity of the sample. In the Meissner state, as long as the sample size is much larger than the London penetration depth and $H \ll H_{c1}$ where H_{c1} is the lower critical field, one has $-4\pi M/H = V_m/(1-D)$, where V_m is the superconducting volume fraction and D is the demagnetization factor. If V_m is assumed to be 1 and independent of field orientation, one obtains $D_{\parallel c} \approx 0.76$ and $D_{\perp c} \approx 0.12$ for this crystal. The D values can be independently estimated from the sample geometry. If an ellipsoid of revolution is used to approximate our sample shape with the dimensions given in Sec. II, we calculate $D_{\parallel c} \approx 0.72$ and $D_{\perp c} \approx 0.14$, which are in good agreement with those found above. This agreement indicates that $V_m \approx 1$, i.e.,

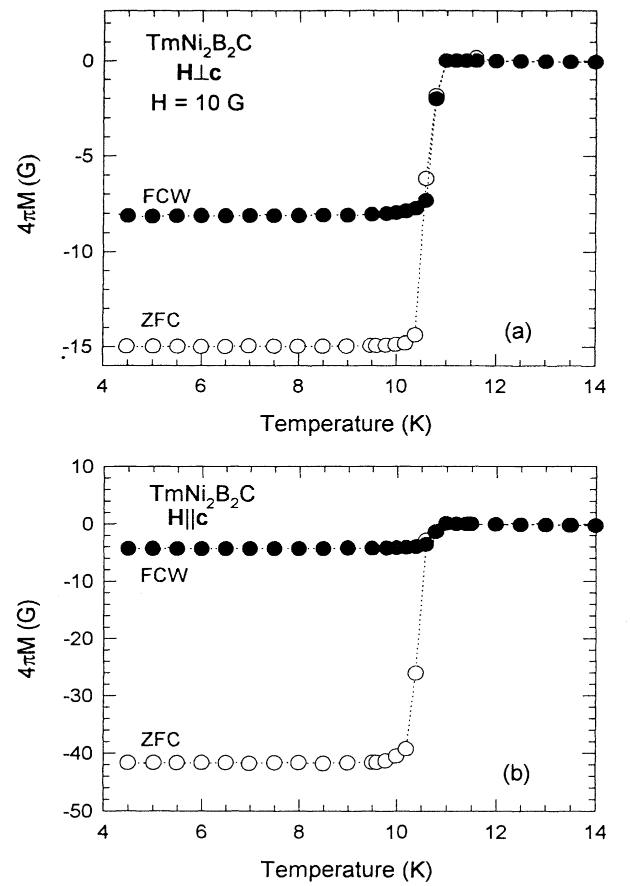

FIG. 1. Superconducting state volume magnetization M versus temperature for a single crystal of $TmNi_2B_2C$ in an applied magnetic field of 10 G: (a) **H**⊥**c**; (b) **H**||**c**. Both ZFC (open circles) and FCW (filled circles) data are shown for each orientation of **H**.

that our crystal is fully superconducting. The data below are not corrected for the demagnetization factors because the demagnetization effects in the high-field data are negligible. In order to examine the superconducting properties of $TmNi_2B_2C$ at higher fields, it is first necessary to characterize the magnetic response of the Tm sublattice. After the next section describing the normal-state magnetization, we will return to analysis of the superconducting magnetization.

B. Normal-state magnetization

The magnetic susceptibilities, $\chi \equiv M/H$, as a function of temperature for 12 K $\le T \le$ 300 K in an applied field of 10 kG, are plotted in Fig. 2(a) for both field orientations. It is noted that the $M(H)$ data for $T > 10$ K are linear in H for fields less than 10 kG (see Fig. 3). An anisotropy, with larger $M(T)$ for **H**∥**c** than for **H**⊥**c**, exists in the whole temperature range between the two orientations, which increases as the temperature decreases. Figure 2(b) shows the $1/\chi$ versus T data together with a calculated powder averaged one ($\chi_{avg} = 2\chi_{H\perp c}/3 + \chi_{H\parallel c}/3$). The data above ~200 K for both field orientations show a Curie-Weiss behavior,

$$\chi = \frac{C}{T-\theta} = \frac{N\mu_{eff}^2}{3k_B(T-\theta)} , \quad (1)$$

where C is the Curie constant, θ is the Weiss temperature, N is the number of Tm^{+3} ions, and μ_{eff} is the effective magnetic moment per formula unit. From the slope of $1/\chi(T)$ for 200 K $\le T \le$ 300 K, μ_{eff} of the Tm^{+3} ion is found to be $(7.63\pm0.02)\mu_B$ and $(7.51\pm0.03)\mu_B$ for **H**⊥**c** and **H**∥**c**, respectively. These values are both in good agreement with the theoretical value of $\mu_{eff} = 7.57\mu_B$ for the Hund's Rule ground state of the isolated Tm^{+3} ion. The Weiss temperatures are found to be $\theta_\perp \approx (-36.0\pm0.6)$ K and $\theta_\parallel \approx (20.8\pm0.3)$ K for **H**⊥**c** and **H**∥**c**, respectively. Below ~150 K, the $1/\chi(T)$ data start to deviate from the linear-T dependence in opposite ways for the two applied field directions as can be seen in Fig. 2(b), indicating changes in the μ_{eff} values with decreasing T in this low-temperature range. In Fig. 2(b), the powder averaged susceptibility shows a linear $1/\chi_{avg}$ vs T behavior to much lower temperatures (~2 K), effectively concealing any sign of the underlying anisotropy. The

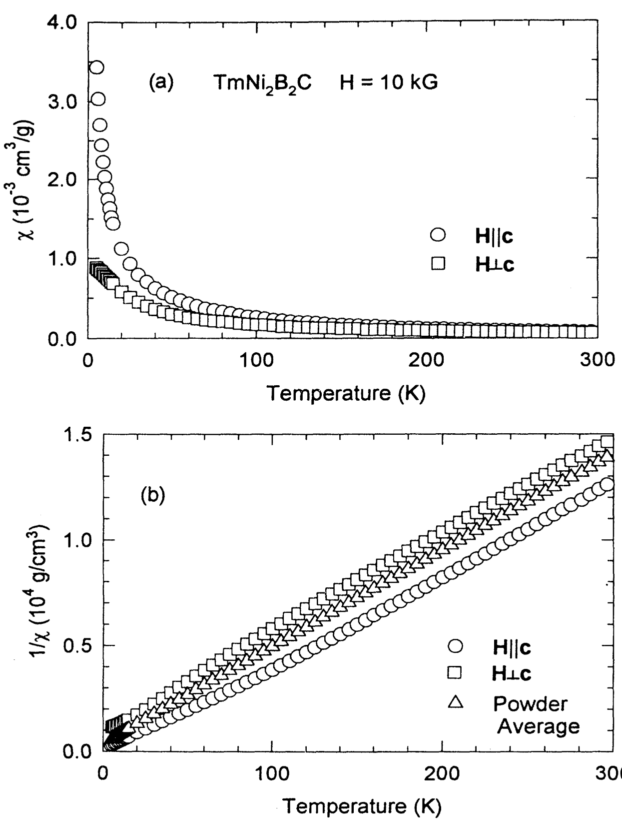

FIG. 2. (a) Magnetic susceptibility χ versus temperature for a single crystal of $TmNi_2B_2C$ in an applied magnetic field $H = 10$ kG for **H**⊥**c** (squares) and for **H**∥**c** (circles), (b) $1/\chi$ from the data in (a) and the powder average, $1/\chi_{avg} = 1/(2\chi_{\perp c}/3 + \chi_{\parallel c}/3)$ (triangles), versus temperature.

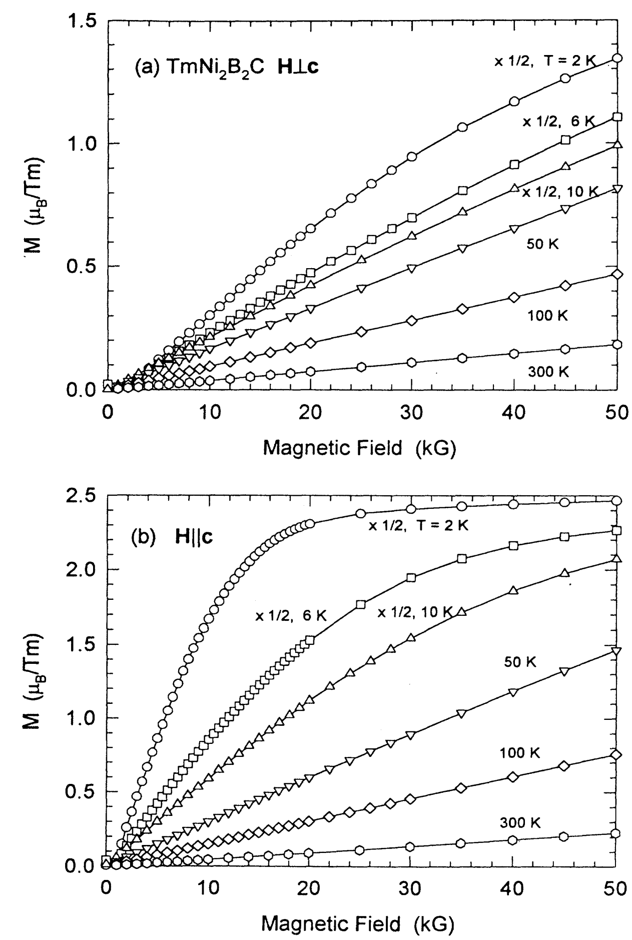

FIG. 3. Magnetization M versus applied magnetic field for a single crystal of $TmNi_2B_2C$: (a) **H**⊥**c**, (b) **H**∥**c**. Note that the magnitude of the magnetization at $T = 2$, 6, and 10 K is scaled by a factor of 0.5 for clarity.

effective moment of this powder average is $\mu_{\rm eff}=(7.54\pm0.02)\mu_B$, slightly lower than the value $\mu_{\rm eff}=7.7\mu_B$ measured on a powder sample,[6] and the Weiss temperature is $\theta_{\rm avg}=(-11.6\pm0.4)$ K. The observation of free-ion-like behavior in $1/\chi_{\rm avg}(T)$ is common even in systems where large anisotropy is present due to crystalline electric-field (CEF) effects, as observed, for example, in most of the $Ln\mathrm{Rh_4B_4}$ compounds[11] as well as in $\mathrm{HoNi_2B_2C}$ (Ref. 8) and the other $R\mathrm{Ni_2B_2C}$ compounds.[12] The CEF effects in $\mathrm{TmNi_2B_2C}$ crystals were also observed in specific-heat measurements on a single crystal from the same batch as the one used in this study, where a splitting of 39 ± 1 K between the ground levels and the next excited states was estimated.[7]

The anisotropic magnetization of single crystal $\mathrm{TmNi_2B_2C}$ most likely comes mainly from the CEF splitting of the $J=6$ ground multiplet of the Tm^{+3} ion. The CEF Hamiltonian for the tetragonal point symmetry ($I4/mmm$) of the Tm^{+3} ion can be written as[13]

$$H_{\rm CEF}=B_2^0O_2^0+B_4^0O_4^0+B_4^4O_4^4+B_6^0O_6^0+B_6^4O_6^4\ , \quad (2)$$

where O_n^m are Stevens operators and B_n^m are constants to be determined experimentally. In general, the field direction in which the susceptibility is largest is determined by the sign of B_2^0. The value of B_2^0 can be calculated from the difference between $\theta_\perp$ and $\theta_\parallel$ using the expression[14]

$$B_2^0=\frac{10}{3(2J-1)(2J+3)}(\theta_\perp-\theta_\parallel)\ . \quad (3)$$

Using the above values of $\theta_\perp$ and $\theta_\parallel$, Eq. (3) gives a value of B_2^0 of (-1.15 ± 0.02) K for $\mathrm{TmNi_2B_2C}$. The point-charge model predicts a change in sign of B_2^0 from the Ho^{+3} ion to the Tm^{+3} ion within an isostructural series such as $R\mathrm{Ni_2B_2C}$ (provided the CEF does not change dramatically). Initial calculations of the CEF parameters for Ho^{+3} give $B_2^0\approx+0.61$ K,[12] which indeed shows a change in sign from the value for Tm^{+3}. Equation (3) and therefore the B_2^0 for $\mathrm{TmNi_2B_2C}$ are derived based on the assumption of uncoupled ions. It should serve as a starting point for more detailed CEF calculations. The sign of B_2^0 for $\mathrm{TmNi_2B_2C}$ predicts that the magnetic easy axis is along **c**, which is consistent with the observed anisotropy in the relative magnitudes of $\mathbf{M}_{\parallel c}$ for **H**$\parallel$**c** and $M_{\perp c}$ for **H**$\perp$**c** shown in Fig. 2. The predicted easy axis for $\mathrm{HoNi_2B_2C}$ and $\mathrm{TmNi_2B_2C}$ based on signs of B_2^0 are in accord with the respective directions of the ordered moments found from recent neutron-diffraction experiments.[15–17]

Typical $M(H)$ isotherm data for $\mathrm{TmNi_2B_2C}$ are shown in Figs. 3(a) for **H**$\perp$**c** and 3(b) for **H**$\parallel$**c** at several different temperatures. For both field orientations, the magnetization is linear in the applied field H for temperatures above 50 K. While weak nonlinearity develops with decreasing T for **H**$\perp$**c**, the $M(H)$ data for **H**$\parallel$**c** show strongly nonlinear behavior below 10 K, leading to a saturation of the Tm^{+3} magnetic moments at $T=2$ K for $H>20$ kG. This saturation moment is close to $5.0\mu_B$ for $H=50$ kG, significantly smaller than the value of $7.57\mu_B$ for an isolated free Tm^{+3} ion. This is likely due to CEF effects because the ground state of the Tm^{+3} ion in a tetragonal CEF is expected to be an admixture of angular momentum eigenstates of $J=6$. The $M(H)$ data at $T=2$ and 6 K (below T_c) for both **H**$\perp$**c** and **H**$\parallel$**c** will be discussed in Sec. III D.

Figure 4 shows the $M(T)/H$ data as a function of temperature ($4\ \mathrm{K}\le T\le 80$ K) for **H**$\parallel$**c** and $H=1$ kG. Above $T\approx10.5$ K, $M(T)/H$ shows Curie-Weiss behavior due to the paramagnetic Tm^{+3} moments. Below $T\approx10.5$ K, an additional diamagnetic signal reduces the paramagnetic signal. Below $T\approx7$ K, the data become field history dependent with the ZFC $M(T)/H$ data being lower than the FCW $M(T)/H$ data. This behavior is consistent with the existence of type-II superconductivity below $T_c\approx10.5$ K, with reversible behavior between 7 K and T_c. Therefore, the sharp peak in Fig. 4 at $T\approx10.5$ K is considered as the onset of superconductivity. This interpretation is also consistent with resistivity measurements in external magnetic field where the resistivity starts to drop near the same temperature for similar field values.[6]

The $M(T)$ has been measured for $2\ \mathrm{K}\le T\le 80$ K for both **H**$\parallel$**c** and **H**$\perp$**c** with several different fields between 1 and 15 kG. For **H**$\parallel$**c**, the $M(T)/H$ data are independent of H for $11\ \mathrm{K}\le T\le 80$ K and can be fitted by the equation, $\chi_{\parallel c}(T)[\equiv M(T)/H]=C/(T-\theta)+\chi_0$, yielding $C=(2.33\pm0.05)\times10^{-2}$ cm^3 K/g, $\mu_{\rm eff}=7.72\mu_B$/Tm, $\theta=(-1.73\pm0.1)$ K, and $\chi_0=(5.1\pm0.2)\times10^{-5}$ cm^3/g (see dotted line in Fig. 4). This form of $\chi_{\parallel c}(T)$ will be used for the subtraction of the paramagnetic contribution from the observed $M(T,H)$ data to examine the field dependence of superconducting magnetization M_s, i.e., $M_{s\parallel}(T,H)=M(T,H)-\chi_{\parallel c}(T)H$. For **H**$\perp$**c**, the $M(T)/H$

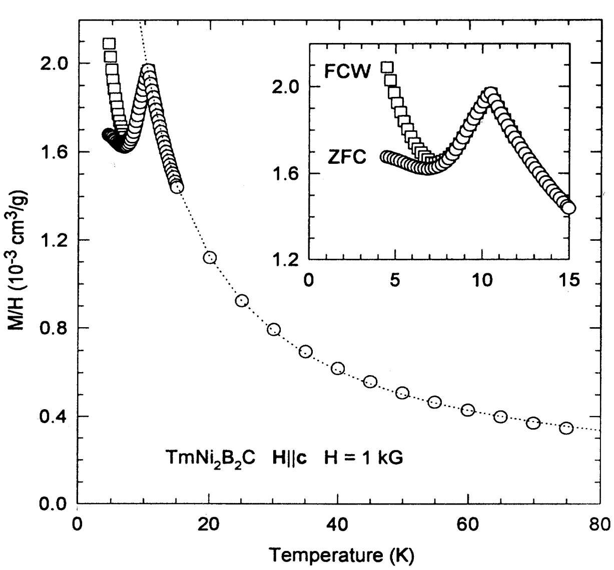

FIG. 4. Magnetization divided by applied magnetic field (M/H) versus temperature for a single crystal of $\mathrm{TmNi_2B_2C}$ with $H=1$ kG and **H**$\parallel$**c**. ZFC (circles) and FCW (squares) data are shown. The dotted line is a Curie-Weiss fit to the data between 11 and 80 K. Inset: Expanded plot of the data below 15 K.

data are field dependent. Therefore, for **H**⊥**c**, $M_{\perp c}(T)$ due to the Tm^{+3} ions was calculated at each field by fitting the data for 11 K $\leq T \leq$ 80 K to a Curie-Weiss form, plus a constant. Subtracting the resultant $M_{\perp c}(T)$ from $M(T,H)$ gives $M_{s\perp}(T,H)$, in a similar manner as for $M_{s\parallel}(T,H)$. It should be noted that we expect such subtractions to be more accurate for $T \approx T_c$ than for $T \ll T_c$ since the Tm^{+3} magnetization contribution will, in reality, have a more complex form than a simple Curie-Weiss temperature dependence, primarily due to saturation effects and the small splitting of the lowest-lying CEF levels.

C. Superconducting state magnetization

After subtracting the paramagnetic magnetization of the Tm^{+3} ions from the observed $M(H,T)$ data, as described in the previous section, the diamagnetic superconducting component of the magnetization M_s is obtained and is plotted in Figs. 5 and 6 for **H**⊥**c** and **H**∥**c**, respectively. For clarity only the M_s data in the reversible region are presented here. As shown in Fig. 5(a) with the full scale of $4\pi M_s = -100$ G, there are clear onsets of diamagnetism for all fields shown in the plot, indicating high sample quality and negligible superconducting fluctuation effects which are commonly seen in high-T_c cuprate superconductors.[18] The diamagnetic magnetization curve shifts to lower temperature and the slopes of the M_s versus T curves seem to gradually decrease as the applied field is increased. This is similar to the behavior of most conventional superconductors including YNi_2B_2C.[10] The expanded plot in Fig. 5(b) shows that the data are nearly linear in T near T_c and have nearly the same slope for a wide region of field. As shown in Fig. 6, a similar linear behavior is also observed for **H**∥**c** in the reversible superconducting region except for $H = 10$ kG. The broadened $M(T)$ for $H = 10$ kG may be due to superconducting critical fluctuation effects because the fluctuation regime broadens with applied magnetic field as observed in the high-T_c superconductor $YBa_2Cu_3O_{7-\delta}$.[19] The upturns with decreasing T, seen in Fig. 5(b) for **H**⊥**c** = 13 and 15 kG, are believed to come from inaccuracy in our subtraction of the Tm^{+3} sublattice contribution to $M(H,T)$. This inaccuracy is likely due mainly to the CEF splitting of $J = 6$ multiplet because the properties of the lowest lying CEF levels become more important as the temperature decreases. This is qualitatively in agreement with our initial calculations of the Tm^{+3} CEF energy levels, which predict two nearly degenerate ground singlets with an energy splitting of less than 2 K, with the next higher level above 17 K.[12]

In the reversible (H,T) region near $H_{c2}(T)$, the Ginzburg-Landau (GL) theory predicts[20]

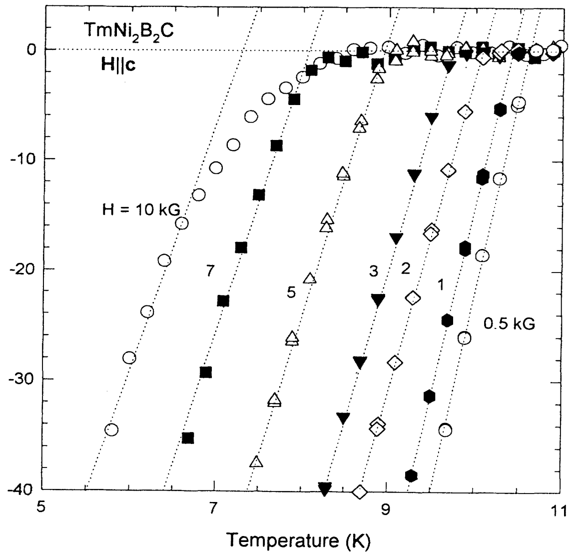

FIG. 6. Superconducting component M_s of the magnetization for **H**∥**c** versus temperature, in the reversible temperature ranges, for $H = 0.5$, 1, 2, 3, 5, 7, and 10 kG.

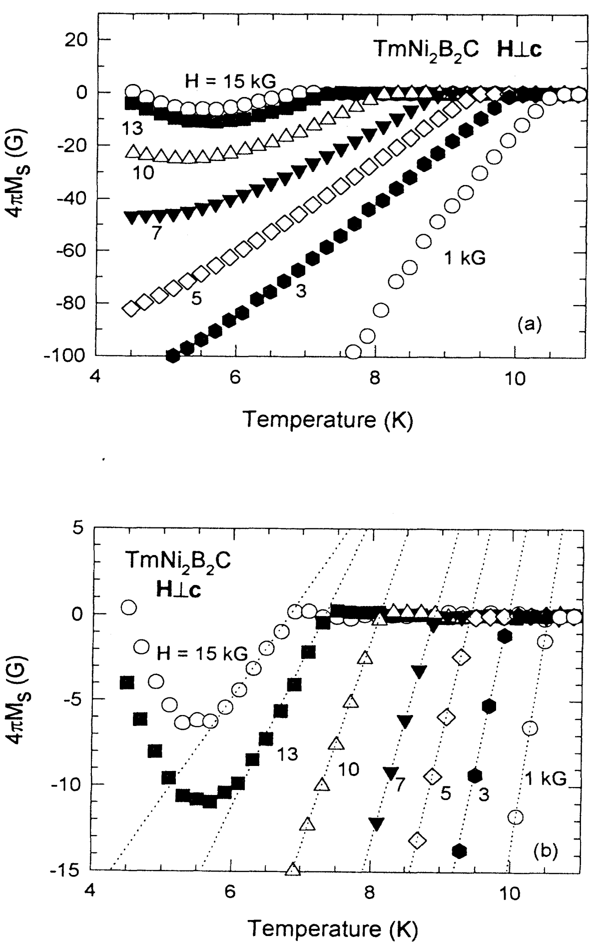

FIG. 5. Superconducting component M_s of the magnetization for **H**⊥**c** versus temperature, in the reversible temperature ranges. (a) Data taken at $H = 1$, 3, 5, 7, 10, 13, and 15 kG. (b) Data in (a) shown on an expanded M_s scale.

$$-4\pi M_s = \frac{H_{c2}(T) - H}{(2\kappa^2 - 1)\beta_A} , \tag{4}$$

where κ is the GL parameter and $\beta_A = 1.16$ is a constant. Since H_{c2} is linear in T for $T \approx T_c$,[20] one should obtain a linear dependence of M_s on T near T_c, as observed for the reversible data in Figs. 5(b) and 6. Extrapolating these linear dependencies to $M_s = 0$ yields $H_{c2}(T) = H$. The H_{c2} values determined here are plotted in Fig. 8 below as open symbols.

For fields higher than those shown in Figs. 5 and 6, M_s is difficult to extract directly from the observed $M(H,T)$ data because M_s becomes very small compared with the contribution of the Tm^{+3} ions. Therefore, we have determined H_{c2} from plots of the point-by-point derivative of M with respect to $H (\equiv \Delta M/\Delta H)$ from the data in Fig. 3; examples of such $\Delta M/\Delta H$ versus H data at $T = 2$ and 6 K for **H**⊥**c** and **H**∥**c** are plotted in Figs. 7(a) and 7(b), respectively. They show clear slope changes for both field orientations at H_{c2}, consistent with Eq. (4), where $\Delta M/\Delta H$ for $H < H_{c2}$ is larger than $\Delta M/\Delta H$ for $H > H_{c2}$.

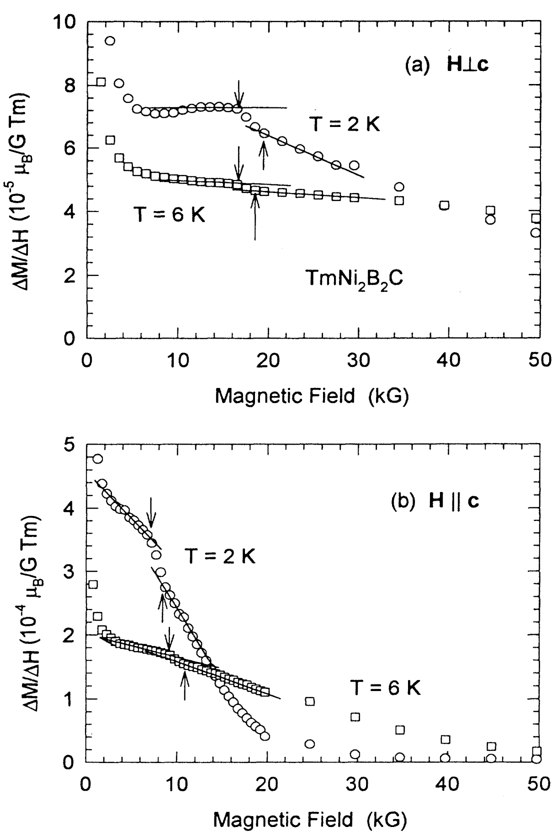

FIG. 7. Derivative of magnetization with respect to applied magnetic field ($\Delta M/\Delta H$) versus magnetic field for the data in Figs. 3(a) and 3(b) for **H**⊥**c** (a) and **H**∥c (b), respectively. The lines are drawn before and after the slope change of $\Delta M/\Delta H$ and arrows indicate the upper and lower limits of the upper critical fields H_{c2}, which are defined as the onsets of the deviations from the lines.

The upper and lower limits of H_{c2} are given by the construction and arrows shown in Fig. 7.

D. Superconducting parameters

The results for $H_{c2}(T)$ from $M_s(T)$, Figs. 5 and 6, and $\Delta M/\Delta H$, such as in Fig. 7, have been plotted in Fig. 8 for **H**∥**c** and **H**⊥**c**. The values of $H_{c2}^{\perp c}$ for **H**⊥**c** from M_s vs T and from $\Delta M/\Delta H$ agree well in the temperature range of overlap, 7 K $\le T \le$ 9 K. The $H_{c2}^{\perp c}(T)$ data increase almost linearly with decreasing T for $T \ge 6$ K, saturate for 3 K $\le T \le$ 6 K and decrease on further cooling. In other words, $H_{c2}^{\perp c}(T)$ shows a broad maximum near 4 K and appears to be suppressed as T approaches T_N. For **H**∥**c**, and $H_{c2}^{\parallel c}(T)$ data also exhibit a linear increase with decreasing T, but they deviate from the linear behavior at higher T (≈ 8 K) than for **H**⊥**c**. These $H_{c2}(T)$ data are in qualitative agreement with $H_{c2}(T)$ data from magnetoresistance measurements on a single crystal grown by the same method as the one studied here.[21] Significant anisotropy in $H_{c2}(T)$ starts to develop below 8 K and $H_{c2}^{\perp c}$ becomes nearly two times larger than H_{c2}^{c} below 6 K. Several characteristic features in $H_{c2}(T)$ of $TmNi_2B_2C$ can be pointed out here. First, the overall anisotropy in $H_{c2}(T)$, i.e., $H_{c2}^{\perp c} > H_{c2}^{\parallel c}$, is consistent with the magnetic anisotropy, $\chi_{H\parallel c} > \chi_{H\perp c}$, in the normal state (Fig. 2), indicating that the conventional magnetic pair-breaking mechanism contributes to this observed anisotropy. Second, for both **H**∥**c** and **H**⊥**c**, $H_{c2}(T)$ is suppressed as T approaches T_N with a broad maximum above T_N, which is common in antiferromagnetic superconductors[9] and consistent with resistivity measurements on polycrystalline $TmNi_2B_2C$.[6] Thus the suppression of H_{c2} below 6 K is attributed to the interplay between the magnetism of

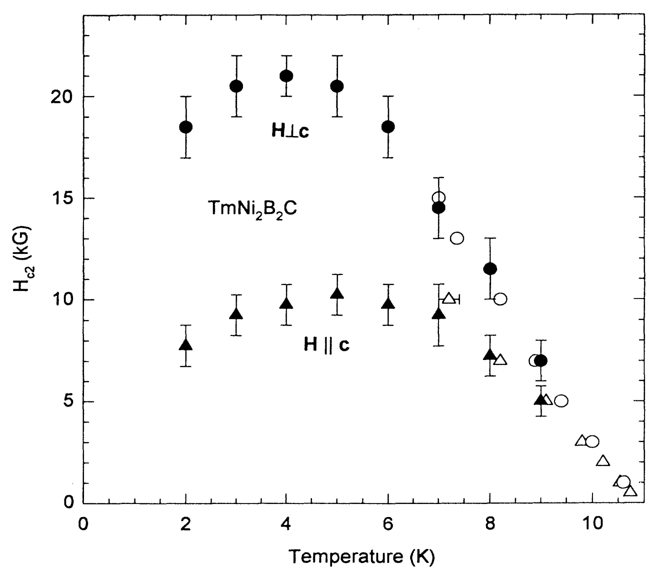

FIG. 8. Upper critical magnetic field H_{c2} versus temperature determined from $M_s(T)$ vs T for **H**⊥**c** (open circles) and **H**∥c (open triangles), or determined from $\Delta M/\Delta H$ vs H for **H**⊥**c** (filled circles) and **H**∥**c** (filled triangles).

the Tm^{+3} ions and superconductivity. The broad maxima in $H_{c2}(T)$ in $TmNi_2B_2C$ contrast with the sharp anomalies in (Ho,Er)Ni_2B_2C near T_N.[8,22] In these respects, the $H_{c2}(T)$ in $TmNi_2B_2C$ is similar to the $H_{c2}(T)$ in the ternary superconductor $ErMo_6S_8$.[23] It is likely that the round maximum and decrease in H_{c2} of $TmNi_2B_2C$ is not directly related to the AF ordering at $T_N=1.5$ K but to the increasing Tm sublattice magnetization at H_{c2} with decreasing temperature. Third, the anisotropy in H_{c2} below 6 K ($H_{c2}^{\perp c}/H_{c2}^{\parallel c}\approx 2$) is significantly larger compared with those of (Ho,Er)Ni_2B_2C,[8,22] although the magnetic anisotropy in the normal state of $TmNi_2B_2C$ is less than in (Ho,Er)Ni_2B_2C. It should be noted that the anisotropy in $H_{c2}(T\geq T_N)$ increases as the ratio T_N/T_c decreases.

From the $H_{c2}(T)$ data in Fig. 8, $dH_{c2}^{\perp c}/dT$ for $\mathbf{H}\perp\mathbf{c}$ and $dH_{c2}^{\parallel c}/dT$ for $\mathbf{H}\parallel\mathbf{c}$ near T_c were determined to be (-3.6 ± 0.2) kG/K and (-2.8 ± 0.2) kG/K, respectively. Using Eq. (4), the κ values were derived to be $\kappa_{ab}=7.7\pm0.4$ for $\mathbf{H}\perp\mathbf{c}$ and $\kappa_c=6.3\pm0.3$ for $\mathbf{H}\parallel\mathbf{c}$; thus $TmNi_2B_2C$ is a type-II superconductor. Using the relation $H_{c2}(0)\approx -0.69T_c(dH_{c2}/dT)_{T_c}$,[24] the extrapolated $H_{c2}(0)$ is estimated to be (27.2 ± 1.5) kG for $\mathbf{H}\perp\mathbf{c}$ and (21.2 ± 1.5) kG for $\mathbf{H}\parallel\mathbf{c}$. The coherence length ξ is then found from $H_{c2}(0)=\phi_0/(2\pi\xi^2)$ to be (110 ± 3) Å and (124 ± 5) Å and the extrapolated penetration depth $\lambda(0)$ to be (850 ± 60) Å and (780 ± 70) Å for $\mathbf{H}\perp\mathbf{c}$ and $\mathbf{H}\parallel\mathbf{c}$, respectively. The anisotropy factor γ, defined as $\gamma=(dH_{c2}^{\parallel c}/dT|_{T_c})/(dH_{c2}^{\perp c}/dT|_{T_c})$, is 1.29 ± 0.16, close to one, in spite of the large anisotropy in the paramagnetic normal-state susceptibility above T_c. This value indicates that $TmNi_2B_2C$ is a nearly isotropic superconductor like YNi_2B_2C,[10] in contrast to the highly anisotropic copper-oxide superconductors with γ values of $\sim$4–55.[25] These equations ignore the effect of the AF ordering at $T_N=1.5$ K and therefore should be treated as first estimates of these values. For example, $H_{c2}(0)$ for $\mathbf{H}\parallel\mathbf{c}$ is expected from Fig. 8 to be much smaller than the above estimation. The superconducting parameters are listed in Table I, together with the ones for YNi_2B_2C and $ErNi_2B_2C$ for comparison.

IV. SUMMARY AND CONCLUSIONS

Using a flux growth method, single crystals of $TmNi_2B_2C$ were successfully grown with masses up to 700 mg and dimensions up to 1 cm$\times$1 cm$\times$0.1 cm. The 12 mg single crystal of $TmNi_2B_2C$ used in this study gives a sharp superconducting transition at $T_c=10.8$ K (midpoint) for $H=10$ G. The $\chi(T)$ above T_c shows an anisotropy in the normal state with the larger magnetization for $\mathbf{H}\parallel\mathbf{c}$ whereas other $Ln$$Ni_2B_2C$ (Ln = Ho, Dy, and Tb) compounds have the larger magnetization for $\mathbf{H}\perp\mathbf{c}$. This is consistent with the negative sign of $B_2^0=(-1.15\pm0.02)$ K for $TmNi_2B_2C$ found here, based on the difference in Weiss temperatures $(\theta_\perp-\theta_\parallel)$. Although the slopes of $1/\chi$ versus T for both orientations are very close to the free ion prediction at high temperatures ($T>150$ K), deviations develop below $\sim$150 K, attributed to CEF effects. On the other hand, the powder averaged $\chi_{avg}(T)$ shows a Curie-Weiss law with an effective moment near the free-ion value over the whole temperature range 2 to 300 K and with $\theta_{avg}=(-11.6\pm0.4)$ K. Most of these anisotropic features can be understood qualitatively as CEF effects.

In the superconducting state, the GL theory describes the data well in the reversible region $H\approx H_{c2}(T)$. The superconducting parameters are summarized in Table I, and are similar to those of YNi_2B_2C and $ErNi_2B_2C$, also listed in Table I. The anisotropy factor near T_c is found to be $\gamma=1.29\pm0.16$, showing that $TmNi_2B_2C$ is a nearly isotropic superconductor in this temperature regime in spite of the anisotropy in the normal state. This is attributed both to the weak overlap of the conduction electrons with the Tm^{+3} local magnetic moments and to the relatively large difference between T_c and T_N, where the ratio $T_N/T_c\approx 1.5/11$. Above $H\sim 10$ kG, the nonlinear behavior of the $M(H)$ data, due to the Tm^{+3} ions, causes difficulties in determining $H_{c2}(T)$ using the GL theory. The derivative of $M(H)$ with respect to $H(\equiv\Delta M/\Delta H)$ exhibits a clear slope change at H_{c2}, allowing the determination of $H_{c2}(T)$ even for $H>10$ kG, which is in nice agreement with the $H_{c2}(T)$ dependences determined by GL theory and the $M(T)$ data in the overlapping temper-

TABLE I. Superconducting parameters for magnetic fields parallel and perpendicular to the c axis in crystals of $TmNi_2B_2C$, $ErNi_2B_2C$, and YNi_2B_2C. The values of $\lambda(0)$, $\xi(0)$, and $H_{c2}(0)$ are extrapolated to $T=0$ from near T_c, and can be significantly different from the actual values in each compound (see text, Sec. III D). κ: GL parameter, γ: anisotropy factor, defined as $(dH_{c2}^{\parallel c}/dT|_{T_c})/(dH_{c2}^{\perp c}/dT|_{T_c})$, ξ: coherence length, λ: penetration depth.

	$dH_{c2}/dT\|_{T_c}$ (T/K)	κ	γ	$H_{c2}(0)^a$ (kG)	$\xi(0)^a$ (Å)	$\lambda(0)^a$ (Å)	Ref.
YNi_2B_2C	~ -0.32	~ 14.5		~ 32	~ 110	~ 1500	10
$TmNi_2B_2C$ $\mathbf{H}\parallel\mathbf{c}$	-0.28 ± 0.02	6.3 ± 0.3	1.29 ± 0.16	21.2 ± 1.5	124 ± 5	780 ± 70	This work
$\mathbf{H}\perp\mathbf{c}$	-0.36 ± 0.02	7.7 ± 0.4		27.2 ± 1.5	110 ± 3	850 ± 60	
$ErNi_2B_2C$ $\mathbf{H}\parallel\mathbf{c}$	-0.26 ± 0.02	8.8 ± 1.2	1.31 ± 0.17	19.1 ± 1.5	131 ± 6	1160 ± 210	22
$\mathbf{H}\perp c$	-0.20 ± 0.01			14.7 ± 0.7	150 ± 4		

[a]Extrapolated to $T=0$ from just below T_c.

ature range. For $T \leq 6$ K, $H_{c2}(T)$ is more anisotropic than near $T_c(H=0)=10.5$ K: $H_{c2}^{\perp c} \approx 2H_{c2}^{\parallel c}$. The observed sign of the anisotropy $H_{c2}^{\perp c} - H_{c2}^{\parallel c}$ has the same sign as $M^{\parallel c} - M^{\perp c}$, suggesting that the depression of H_{c2} increases monotonically with the Tm sublattice magnetization. The H_{c2} values for both $\mathbf{H} \perp \mathbf{c}$ and $\mathbf{H} \parallel \mathbf{c}$ appear to decrease as T decreases below ~ 5 K, which is an indication that the maximum in $H_{c2}(T)$ of $TmNi_2B_2C$ is related to the increasing Tm sublattice magnetization of H_{c2} with decreasing temperature, rather than AF fluctuations above T_N. Identification of the magnetic state below T_N and more measurements down to and below T_N will be needed to explain more clearly the anomalous behavior in $H_{c2}(T)$.

ACKNOWLEDGMENTS

Ames Laboratory is operated for the U.S. Department of Energy by Iowa State University under Contract No. W-7405-Eng-82. This work was supported by the Director for Energy Research, Office of Basic Energy Sciences.

[1]R. Nagarajan, Chandan Mazumdar, Zakir Hossain, S. K. Dhar, K. V. Gopalakrishnan, L. C. Gupta, C. Godart, B. D. Padalia, and R. Vijayaraghavan, Phys. Rev. Lett. **72**, 274 (1994); **73**, 211(E) (1994).

[2]R. J. Cava, H. Takagi, H. W. Zandbergen, J. J. Krajewski, W. F. Peck, Jr., T. Siegrist, B. Batlogg, R. B. van Dover, R. J. Felder, K. Mizuhashi, J. O. Lee, H. Eisaki, and S. Uchida, Nature (London) **367**, 252 (1994).

[3]H. C. Ku, C. C. Lai, Y. B. You, J. H. Shieh, and W. Y. Guan, Phys. Rev. B **50**, 351 (1994); J. L. Sarrao, M. C. de Andrade, J. Herrmann, S. H. Han, Z. Fisk, M. B. Maple, and R. J. Cava, Physica C **229**, 65 (1994).

[4]B. T. Matthias, E. Corenzwit, J. M. Vandenberg, and H. E. Barz, Proc. Nat. Acad. Sci. **74**, 1334 (1977); J. M. Vandenberg and B. T. Matthias, *ibid.* **74**, 1336 (1977).

[5]T. Siegrist, H. W. Zandbergen, R. J. Cava, J. J. Krajewski, and W. F. Peck, Jr., Nature (London) **367**, 254 (1994).

[6]H. Eisaki, H. Takagi, R. J. Cava, B. Batlogg, J. J. Krajewski, W. F. Peck, Jr., K. Mizuhashi, J. O. Lee, and S. Uchida, Phys. Rev. B **50**, 647 (1994).

[7]R. Movshovich, M. F. Hundley, J. D. Thomson, P. C. Canfield, B. K. Cho, and A. V. Chubukov, Physica C **227**, 381 (1994).

[8]P. C. Canfield, B. K. Cho, D. C. Johnston, D. K. Finnemore, and M. F. Hundley, Physica C **230**, 397 (1994).

[9]For a review, see Ø. Fischer, in *Ferromagnetic Materials,* edited by K. H. J. Buschow and E. P. Wohlfarth (North-Holland, Amsterdam, 1990), Vol. 5, p. 465.

[10]M. Xu, P. C. Canfield, J. E. Ostenson, D. K. Finnemore, B. K. Cho, Z. R. Wang, and D. C. Johnston, Physica C **227**, 321 (1994); M. Xu, B. K. Cho, P. C. Canfield, D. K. Finnemore, D. C. Johnston, and D. E. Farrell, *ibid.* **235–240**, 2533 (1994); E. Johnston-Halperin, J. Fiedler, D. E. Farrell, M. Xu, B. K. Cho, P. C. Canfield, D. K. Finnemore, and D. C. Johnston, Phys. Rev. B **51**, 12 852 (1995).

[11]B. D. Dunlap, L. N. Hall, F. Behroozi, G. W. Crabtree, and D. G. Niarchos, Phys. Rev. B **29**, 6244 (1984).

[12]B. K. Cho, P. C. Canfield, B. N. Harmon, and D. C. Johnston (unpublished).

[13]John L. Prather, U. S. National Bureau of Standards, Monograph No. 19 (1961).

[14]Pierre Boutron, Phys. Rev. B **7**, 3226 (1973).

[15]A. I. Goldman, C. Stassis, P. C. Canfield, J. Zarestky, P. Dervenagas, B. K. Cho, D. C. Johnston, and B. Sternlieb, Phys. Rev. B **50**, 9668 (1994).

[16]T. E. Grigereit, J. W. Lynn, Q. Huang, A. Santoro, R. J. Cava, J. J. Krajewski, and W. F. Peck, Jr. Phys. Rev. Lett. **73**, 2756 (1994).

[17]C. Stassis *et al.* (unpublished).

[18]W. C. Lee, R. A. Klemm, and D. C. Johnston, Phys. Rev. Lett. **63**, 1012 (1989); P. H. Kes, C. J. van der Beek, M. P. Maley, M. E. McHenry, D. A. Huse, M. J. V. Menken, and A. A. Menovsky, *ibid.* **67**, 2383 (1992).

[19]M. B. Salamon, S. E. Inderhees, J. P. Rice, B. Z. Pazol, D. M. Ginsberg, and Nigel Goldenfeld, Phys. Rev. B **38**, 885 (1988).

[20]M. Tinkham, *Introduction to Superconductivity* (Krieger, Malabar, FL, 1980).

[21]D. G. Naugle, K. D. D. Rathnayaka, A. K. Ghatnagar, P. C. Canfield, and B. K. Cho (unpublished).

[22]B. K. Cho, P. C. Canfield, L. L. Miller, D. C. Johnston, W. P. Beyermann, and A. Yatskar, following paper, Phys. Rev. B **52**, 3684 (1995).

[23]M. Ishikawa and Ø. Fischer, Solid State Commun. **24**, 747 (1977).

[24]N. R. Werthamer, E. Helfand, and P. C. Hohenberg, Phys. Rev. **147**, 295 (1966).

[25]D. E. Farrell, C. M. Williams, S. A. Wolf, N. P. Bansal, and V. G. Kogan, Phys. Rev. Lett. **61**, 2805 (1988); D. E. Farrell, S. Bonham, J. Foster, Y. C. Chang, P. Z. Jiang, K. G. Vandervoort, D. J. Lam, and V. G. Kogan, *ibid.* **63**, 782 (1989).